

Application of Computational Fluid Dynamics (CFD) for the Evaluation of Fluid Convective Radial Heat Transfer Parameters in Packed Beds

Mariana T. Zambon,^{†,‡} Daniela A. Asensio,^{†,‡} Guillermo F. Barreto,^{§,⊥} and Germán D. Mazza^{*,†,‡}

[†]Instituto de Investigación y Desarrollo en Ingeniería de Procesos, Biotecnología, y Energías Alternativas, PROBIEN (CONICET-Universidad Nacional del Comahue) and [‡]Departamento de Química, Facultad de Ingeniería, Calle Buenos Aires No. 1400, 8300 Neuquén, Argentina

[§]PROIRQ, Departamento de Ingeniería Química, Facultad de Ingeniería and [⊥]Centro de Investigación y Desarrollo en Ciencias Aplicadas “Dr. J.J. Ronco”, CINDECA (CONICET-Universidad Nacional de La Plata), Calle 47 No. 257, 1900 La Plata, Argentina

ABSTRACT: A model to simulate the behavior of multitubular packed-bed catalytic reactors was recently proposed [Asensio, D. A.; Zambon, M. T.; Mazza, G. D.; Barreto, G. F. *Ind. Eng. Chem. Res.* 2014, 53, 3587–3605]. In particular, the model introduces a heat transfer coefficient h_{wf} that accounts for an unmixed fluid film on the wall and a coefficient h_f between the fluid channels at a distance $D_p/2$ from the wall. Computational fluid dynamics simulations intended to evaluate these parameters are described. Four regular sphere arrays between parallel planes that provide different combinations of wall and core channel voidages (ε_1 and ε_c) were employed. Reynolds and Prandtl numbers ranges were $100 < Re_p < 2000$ and $0.4 < Pr < 3.5$. Calculated values of h_{wf} and h_f are well correlated with those of ε_1 , ε_c , Re_p , and Pr . Results for ε_1 and ε_c values typical of randomly packed beds of low ratio D_t/D_p show good agreement with carefully analyzed data from the literature.

1. INTRODUCTION

The correct evaluation of radial heat transport is crucial to simulate the behavior of multitubular packed-bed catalytic reactors. Small ratios of tube-to-particle diameters (aspect ratio, $N = D_t/D_p$), commonly in the range of $5 < N < 15$, are used in industrial practice to enhance radial heat-transfer rates. Because of the highly nonlinear dependence of catalytic reactions with temperature, and frequently for safety reasons, it has been long ago realized that mathematical simulation of such units should provide radial and axial temperature distributions in the catalytic packed tubes. The paper by Dixon¹ undertakes a critical and up-to-date review of efforts to model radial heat transfer in packed beds. The most frequently employed and studied two-dimensional (2D) model assumes radially uniform axial velocity and void fraction and describes radial heat transfer by means of an also uniform effective thermal conductivity, λ_e . The model, identified here as the standard two-dimensional (S2D) model, further introduces a thermal resistance located just at the wall, which is customarily expressed by its inverse, the wall heat transfer coefficient h_w^S . This coefficient encloses several effects: as the thermal resistance due to an unmixed fluid film against the wall, the impairment of radial dispersion of the fluid close to the wall, and the existence of a single contact point between the wall and particles touching it (as opposed to several contact points between particles that enhance thermal conductive contributions). A number of models have been proposed to correct the S2D model by recognizing that the radial heat-transfer mechanisms are restrained over a certain distance from the wall (of the order of D_p) instead of considering a concentrated resistance just at the wall.¹

A new model of this type, identified as two-region two-dimensional (2R2D) model, has been recently introduced by Asensio et al.² The model intends to disaggregate the effects

lumped in the parameter h_w^S of the S2D model by recognizing in a discrete manner the existence of a well-defined layer of particles that virtually touch the tube wall. This feature is very well-known for monosized spherical particles, and it has also been shown to closely apply in the case of equilateral cylinders.^{3,4} Heat exchange between the particles in this layer and the wall can be correctly evaluated by considering a single contact point provided by each particle. As a consequence of the first particle layer, a zone extended from the wall up to half-particle diameter (the distance at which the particle centers lie) can be identified, which presents a significantly higher voidage (ε_1) than the rest of the bed (ε_c). Axial fluid convection is facilitated in the voids of this zone (wall channel) because of its high permeability, but lateral exchange with the rest of the bed is impaired by very low local voidages close to the $D_p/2$ boundary. This causes a thermal resistance to radial heat exchange within the fluid phase, identified as $1/h_f$ that the model locates just at $D_p/2$ from the wall. A second thermal resistance for the fluid flowing in the wall channel is located just at the wall ($1/h_{wf}$) on account of the unmixed fluid film. The fluid flowing in the wall-channel is characterized by average values of temperature (T_1) and superficial mass velocity (G_1) different to that (G_c) in the remains (core channel) of the bed. The fluid in the core channel is modeled as a pseudocontinuous medium (with an effective radial heat thermal conductivity $\lambda_{ef,c}$), and a similar approach is used to describe the behavior of particles other than those in the first layer. The model discriminates between temperature and composition in the fluid and particles.

Received: July 1, 2014

Revised: November 12, 2014

Accepted: November 14, 2014

Published: November 14, 2014

Asensio et al.² discussed that the evaluation of parameters h_{wf} and h_f is subject to uncertainty; hence, the main goal of this paper is to present a first attempt to estimate such parameters by means of computational fluid dynamics (CFD), from which the ratio G_1/G_c can be also evaluated. CFD has been employed intensively to the study of packed-bed behavior in the last 15 years. A review of efforts until 2005 is provided by Dixon et al.,⁵ while more recent contributions are quoted by Dixon.¹ CFD simulation of catalytic packed-bed reactors at full scale is not yet practical with standard computational resources. The approach that most directly employs CFD information is the model proposed by Behnam et al.⁶ Instead, many CFD studies are devoted to study specific aspects of radial heat transport,⁷⁻¹¹ but no suitable information is provided to estimate the parameters h_{wf} and h_f of the 2R2D model. To this end, the implementation of CFD on several regular arrays of spheres is presented in section 3. The regression of CFD results to obtain h_{wf} , h_f and G_1/G_c values, their correlation with structural parameters (ϵ_1 and ϵ_c), and Reynolds and Prandtl numbers (Re_p , Pr) is presented in section 4. Although experimental data have been customarily reduced in terms of the S2D model parameter h_w^S , the analysis of existing correlations for this parameter allows the undertaking of some useful comparison with the results introduced here, as presented in section 5.

2. THE 2R2D MODEL FOR FITTING CFD CALCULATIONS

The 2R2D model has been formulated by Asensio et al.² for a cylindrical packed bed in which catalytic reactions inside the spherical particles take place. This paper is concerned with convective contributions to radial heat transfer, and therefore, conductive contribution involving the solid phase and chemical reaction effects are neglected. Besides, packed beds confined between parallel plates, which also act as heat sources at constant temperature T_w , are involved in the CFD calculations discussed in section 3. Figure 1 illustrates the division of the fluid stream into the wall and core channels and radial heat exchange through the fluid phase. A very long bed on the x -coordinate is assumed to avoid boundary effects along this direction.

Under the conditions just described, the solution of the energy conservation equation in the wall and core channels with uniform fluid properties has been given by Zamboni¹² in the form of an infinite series. Here we are interested in large enough values of z when the temperature profile becomes developed. Hence, only the leading term in the series solution has to be considered:

$$T_1(z) = T_w + C \exp\left[-\beta^2 \frac{1}{Pe H} z\right] \left(\cos \beta - \frac{\beta \sin \beta}{Bi_f}\right) \quad (1a)$$

$$T_c(y, z) = T_w + C \exp\left[-\beta^2 \frac{1}{Pe H} z\right] \cos\left(\beta \frac{W - 2y}{W - D_p}\right) \quad (1b)$$

where H is the height of the cell employed in CFD calculations, W is the bed width, C is an integration constant, and β is the smallest positive eigenvalue of the solution calculated by solving

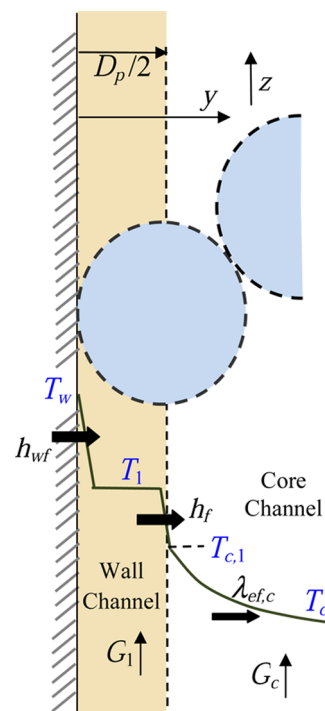


Figure 1. Sketch of the 2R2D model.

$$\begin{aligned} & \beta \tan \beta \left[\beta^2 - (Bi_{wf} + Bi_f) \frac{G_c}{G_1} \frac{(W - D_p)}{D_p} \right] \\ & = Bi_f \left[\beta^2 - Bi_{wf} \frac{G_c}{G_1} \frac{(W - D_p)}{D_p} \right] \end{aligned} \quad (2)$$

The following dimensionless groups have been introduced in eqs 1a, 1b, and 2:

$$\begin{aligned} Bi_f &= \frac{h_f}{\lambda_{ef,c}} \frac{(W - D_p)}{2}; \quad Bi_{wf} = \frac{h_{wf}}{\lambda_{ef,c}} \frac{(W - D_p)}{2}; \\ Pe &= \frac{(W - D_p)^2 c_{pf} G_c}{4H \lambda_{ef,c}} \end{aligned} \quad (3)$$

For the purpose of evaluating the 2R2D model's parameters h_{wf} , h_f and G_1/G_c from CFD calculations, average values on the cell height H (denoted $\langle \bullet \rangle$) will be useful. Starting from the local heat flux at the wall, $Q_w = h_{wf} (T_w - T_1)$,

$$\langle Q_w \rangle = h_{wf} (T_w - \langle T_1 \rangle) \quad (4)$$

From averaging eqs 1a and 1b on H and using eq 4,

$$\langle T_c(y) \rangle = T_w - \frac{\langle Q_w \rangle}{h_{wf}} \frac{\cos\left(\beta \frac{W - 2y}{W - D_p}\right)}{(\cos \beta - \beta \sin \beta / Bi_f)} \quad (5)$$

3. CFD METHODOLOGY

The CFD software allows for the numerical solving of momentum, energy, and mass conservation equations in a given system. A discrete particle simulation of a packed bed has been performed in this work by employing the Academic Research ANSYS-FLUENT code, version 14.0. This mode of CFD application means that the location of each particle in a packed bed, or in a representing part of it, is identified, and the

interstitial fluid volume is discretized in 3D elements for the purpose of solving the underlying conservation equations. Although in general each particle volume can be discretized to account for fluid–solid mass and heat exchange, only the external particle surfaces were meshed in the present case to set the nonslip boundary condition needed to describe the fluid velocity field.

The discrete particle simulation of fixed beds represents a great computational effort. The mesh should be very fine to suitably evaluate the fields of velocity and temperature. Because of this fact, the approach undertaken in this work was to consider packed beds with regular arrays of spheres between parallel flat walls acting as a heat source. Provided that bed entrance and exit effects are disregarded (they should not be important in industrial tubes of very large height-to-particle diameter ratios), regular arrays allow use of cells of relatively low numbers of particles with periodic boundary conditions along the fluid-flow direction.

The simulations are mainly aimed to evaluate the effective thermal parameters of the 2R2D model, h_{wf} and h_p and the ratio of mass superficial velocities G_1/G_c . In randomly packed beds, these parameters should primarily depend on the void fractions in the wall (ϵ_1) and core (ϵ_c) channels. The CFD simulations have been performed on different regular arrays, which provide different levels of such void fractions and also different combination between them. The proper assemblage of the results is then expected to provide a way to estimate h_{wf} , h_p and G_1/G_c in randomly packed beds characterized by proper values of ϵ_1 and ϵ_c .

3.1. Regular Arrays, Mesh Generation, and Range of Operating Conditions. The four regular arrays of spheres employed for CFD simulations are illustrated in Figure 2 along

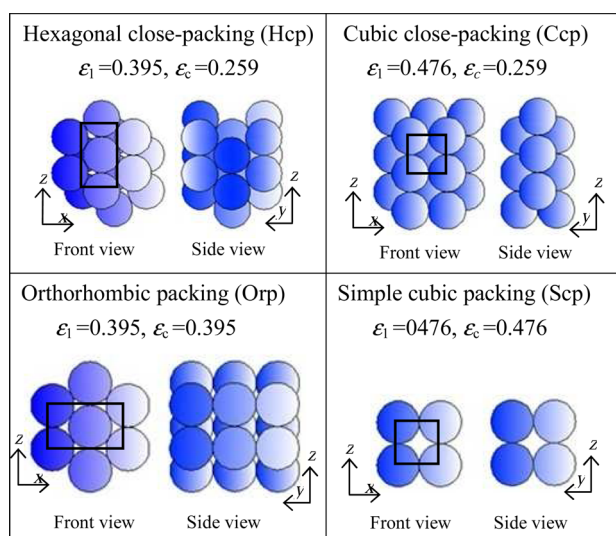


Figure 2. Regular particle arrays. The direction of fluid flow is along coordinate z .

with their acronyms and voidages ϵ_1 and ϵ_c . In Figure 2, the “Front view” plane is parallel to the surfaces containing the bed, which are assumed to be maintained at a uniform temperature T_w . The arrays in Figure 2 provide two levels of ϵ_1 , three levels of ϵ_c , and three levels of the difference ($\epsilon_1 - \epsilon_c$). The fluid-flow direction in the schemes of Figure 2 is that of coordinate z . If the positions of the arrays are maintained and the flow direction is rotated around an axis normal to the plates, the flow will face

different particle configurations. Therefore, simulations were carried out with flow directions as in Figure 2 and rotated 30° for Hcp and Orp and 45° for Ccp and Scp (note that an additional turn with the same angle restores the same configuration as in Figure 2). The values employed for the correlation of h_{wf} , h_p and G_1/G_c were the average from both orientations of the fluid flow.

The sections of the calculation cells parallel to the confining surfaces are illustrated with the rectangles drawn in Figure 2 for a vertical fluid-flow orientation. On the planes normal to the z -axis, periodic boundary conditions were employed. In general, symmetry boundary conditions were employed on the planes normal to the x -axis, except for the Hcp (Figure 2), for which periodic boundary conditions had to be employed. When the z -axis is rotated as defined before, symmetry boundary conditions on the planes normal to the x -axis could be employed for the four arrays.

The number of particles layers along the y -axis, that is, between both confining surfaces, was chosen from a preliminary test in which values of h_{wf} were computed as the number of layers was increased. Values of h_{wf} remain practically constant for five, seven, and nine layers. Thus, seven layers were chosen to obtain the main body of results.

Tetrahedral control volumes were employed for grid generation. It is known that extremely skewed elements arise in the zones surrounding the contact points between particles and between particles and the wall surface, which lead to very low-quality meshing. To avoid this drawback, it is necessary to introduce some geometrical modification to the spherical particles. Four methods to solve the contact-point problem were summarized by Dixon et al.¹³ The “gap” method^{7,14–16} of reducing the sphere diameter in 1% was employed in the present work because of its simplicity. This approach slightly changes the voidage of the arrays, an effect that was not appraised as being significant because of the goal of the present CFD simulations.

For the particle arrays in Figure 2, the resulting values of voidage in the wall and core regions are presented in Table 1 along with averages of the ratio G_1/G_c calculated from simulations in the range of $100 < Re_p < 2000$, which will be used as referential values later on.

Table 1. Porosities and Ratios G_1/G_c (Averaged on $100 < Re_p < 2000$) for Particle Arrays in Figure 2

array	ϵ_c	ϵ_1	G_1/G_c
Hcp	0.282	0.412	2.41
Orp	0.415	0.414	0.84
Scp	0.491	0.492	0.96
Ccp	0.282	0.492	3.07

For mesh validation, grids with different degrees of refinement were tested at $Re_p = 1000$. The coarsest mesh that could adequately reproduce the chosen reference parameter (pressure drop and heat-transfer flux at the wall) was identified and adopted for further simulations. In this way, $1-3 \times 10^6$ control volumes were employed in the calculation cells of the arrays in Figure 2, which allow for evaluation of the flux at the wall within 5% accuracy.

Air properties assumed to be uniform within the calculation cell were mainly used in CFD simulations for different gas-flow rates covering $100 < Re_p < 2000$. Different values of Prandtl numbers in the range of $0.4 < Pr < 3.5$ were tested by changing the thermal conductivity of the fluid. All simulations were

conducted under steady-state conditions and particle size $D_p = 0.01$ m.

Results at $Re_p = 100$ were obtained using laminar calculations, while for the remaining range of Reynolds numbers, the Spalart–Almaras turbulence model was used. Further details about CFD implementation can be found in the work by Zambon.¹²

4. RESULTS AND DISCUSSION

The results for h_{wf} , h_f and G_1/G_c from CFD simulations and their correlations with operating variables will be presented and discussed in the following sections. It is recalled that reported values of all parameters correspond to averages from the two orientations of fluid flow with respect to the arrays of particles (Figure 2), as discussed in section 3.1.

4.1. Heat-Transfer Coefficient h_{wf} . The average value $\langle Q_w \rangle$ on the wall surface of the calculation cell and the mixing cup average temperature $\langle T_1 \rangle$ in the region $0 < y < D_p/2$ (i.e., the wall-channel of the 2R2D model) were evaluated. The heat-transfer coefficient at the wall h_{wf} was then calculated from eq 4.

The results for particle arrays in Figure 2 are illustrated (symbols) in Figure 3 for the whole range of Re_p and $Pr = 0.814$.

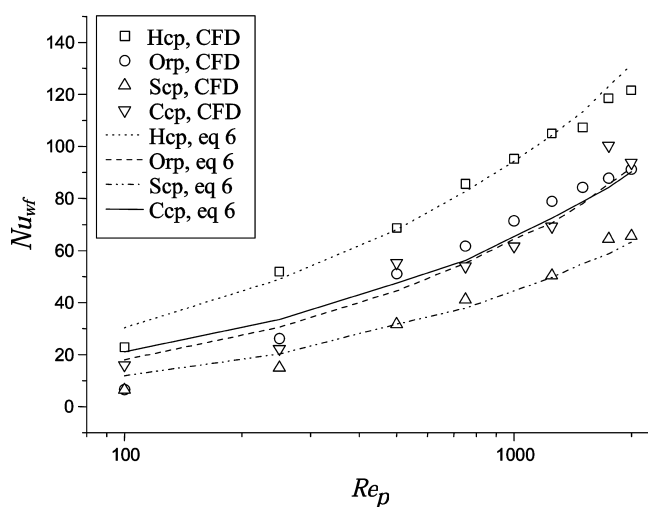


Figure 3. Nu_{wf} versus Re_p values for different particle arrays. $Pr = 0.814$.

The type of array exerts a strong effect on the value of Nu_{wf} . To discriminate the more basic reasons for this behavior, the voidage in the wall channel ε_1 can be considered in first place. The Hcp and Orp show smaller values of ε_1 than do Scp and Ccp (Table 1), and Nu_{wf} values are, on average, larger for the former pair. This trend can then be ascribed to the fact that a low voidage implies that particles in the first layer will obstruct more intensively the fluid flow in the wall channel and avoid the building of a thick boundary layer on the wall surface. On the other hand, Nu_{wf} should depend on the mass superficial velocity in the wall channel G_1 rather than on the overall mass superficial velocity G , on which the overall Re_p value in Figure 1 is based. From the reference values of the ratio G_1/G_c shown in Table 1, it is clear that within the pair Hcp and Orp, G_1 is substantially larger for Hcp at the same G value, which thus explains the larger values of Nu_{wf} . A similar conclusion can be drawn for the pair Scp and Ccp. On the basis of the previous discussion, the following type of expression has been tried to correlate the present results for Nu_{wf}

$$Nu_{wf} = A\varepsilon_1^\alpha Re_{p1}^\beta Pr^\gamma \quad (6)$$

where $Re_{p1} = G_1 D_p / \mu_f$ is the Reynolds number based on G_1 , and A , α , β , and γ are fitting parameters. In practice, values of G_1 can be obtained from G by using eq 8 described in section 4.3. It is recalled that similar sets of results as those presented in Figure 3 were performed for four additional values of Prandtl numbers, which cover the range of $0.4 < Pr < 3.5$ mentioned in section 3.1.

The following modal values of the parameters in eq 6 and their confidence intervals were obtained from a regression analysis of the CFD results:

$$A = 0.285 \pm 0.008, \alpha = -2.4 \pm 0.4, \beta = 0.5 \pm 0.05, \gamma = 0.5 \pm 0.02$$

It is noted that with these modal values, eq 6 predicts $Nu_{wf} \propto (Re_{p1} Pr)^{0.5}$, just as the Penetration model for heat/mass transfer will. Also, a strong effect of ε_1 arises. Values from eq 6 and CFD results show good agreement for the whole range of Re_p values (Figure 3).

Regarding the effect of fluid-flow orientation discussed in section 3.1, it is noted that significant differences in values of Nu_{wf} arise for the Ccp and Scp. In the case of flow orientation as in Figure 2, nearly straight streamlines parallel to the particle strings of these arrays develop with thick boundary layers. On the contrary, when the fluid flow is rotated 45° with respect to the case in Figure 2, the particles offer a frontal obstruction to fluid flow, which enhances the heat-transfer rate and hence increases the Nusselt number at around 100%.

4.2. Heat-Exchange Coefficient h_f . As described in the Introduction, the thermal resistance $1/h_f$ is introduced in the 2R2D model to account for the restrained fluid motion at distances from the wall of around $D_p/2$. For the arrays studied in this work, the “front view” of Orp and Scp in Figure 2 can be interpreted as a cut of the first particle layer by a z,x plane at a distance $y = D_p/2$. The small and close voids hinder the fluid motion. The small y -component of velocity, which is responsible for convective radial heat transport, and the small open area allow for conceiving the thermal resistance $1/h_f$.

The velocity fields provided by CFD simulations are useful to visualize this effect, as it is exemplified in Figure 4. Figure 4, panel a shows a velocity vector plot on a y,z plane tangent to the particle surfaces for Scp at $Re_p = 1000$. The rectangle at the base of the diagram corresponds to the wall surface, and the vectors are colored by the velocity magnitude. The low velocities at positions close to $y = D_p/2$ can be clearly observed. The effect is also evident by comparing the velocity vector plots on x,z planes at $y = D_p/10$, $D_p/2$, and D_p in Figure 4, panel b.

To obtain h_f values, the radial temperature profile in the core region ($y > D_p/2$) averaged on the cell height from the CFD simulations, $\langle T_c(y) \rangle$, was compared to the profile given by the 2R2D model, as given by eq 5. The values $\langle T_c(y) \rangle$ from the CFD calculations were mixing cup averages. The heat-exchange coefficient h_f and the effective conductivity in the core channel $\lambda_{ef,c}$ were used as fitting parameters using the least-squares method.

Before the values of h_f thus obtained are presented, it is worth a discussion of the resulting values of $\lambda_{ef,c}$. The four regular arrays in Figure 2 correspond to series of perfectly ordered sphere-layers parallel to the wall surface; thus, the restriction to fluid flow and hence to radial heat transfer discussed above for the first particle layer at positions around $D_p/2$ from the wall will be found for the second layer at the distance of the plane containing its particle centers, for example, $1.5 D_p$ in the case of Scp and $1.32 D_p$ in the case of Hcp. The situation will be exactly repeated for the third and successive particles layers. The fluid largely flows along parallel channels between each pair of layers with little

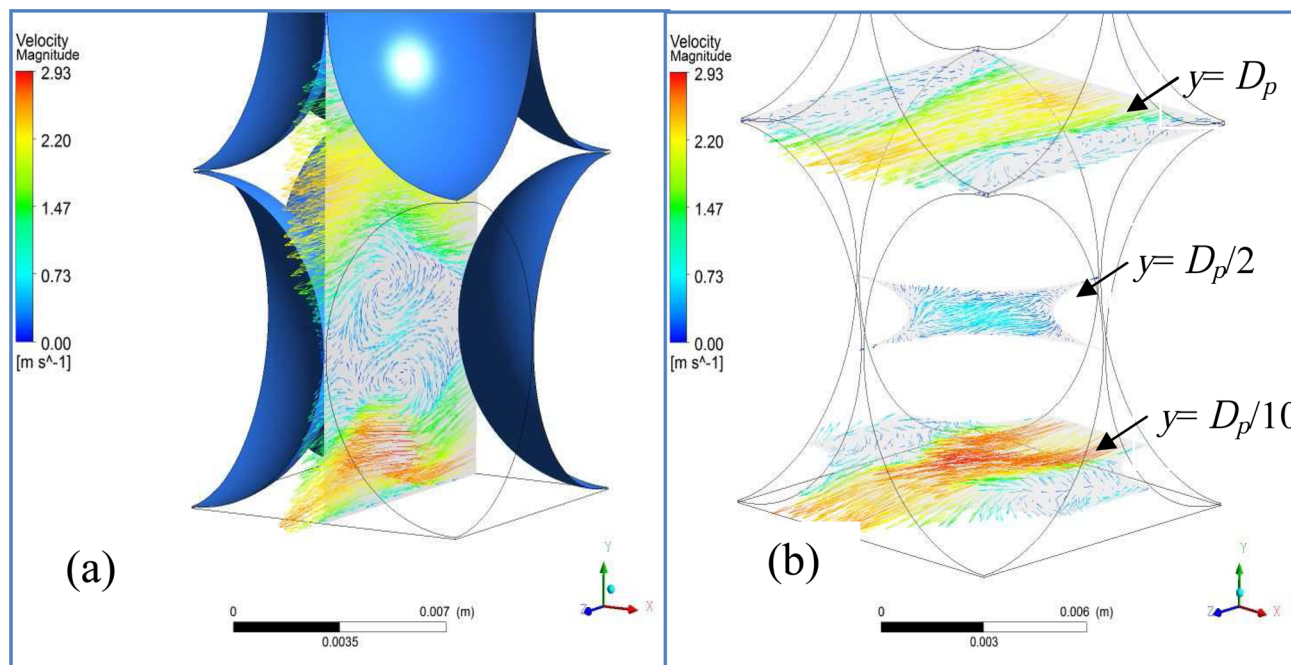


Figure 4. Velocity vectors corresponding to Scp at $Re_p = 1000$ (a) on a z,y plane tangent to particle surfaces and (b) on x,z planes at $y = D_p/10, D_p/2,$ and D_p .

lateral deflection, and as a consequence, the fluid convection contribution to radial heat transfer will be poor on the whole cross-section. Contrariwise, in a randomly packed bed, an identifiable second layer already shows a significant dispersion of the particle centers (as was discussed, e.g., by Asensio et al.²) around the average y -coordinate, a trend that is strengthened deeper inside the bed. In this way, particles effectively act as obstacles for the fluid flow, which has to deviate from generating lateral components of velocity and hence enhances the radial heat transfer. Therefore, small-fitting values of $\lambda_{ef,c}$ were obtained compared to values from literature correlations developed for randomly packed beds. For this reason, values of $\lambda_{ef,c}$ obtained in this study will not be further discussed.

Results of h_f values, expressed in terms of Nu_f numbers, are shown in Figure 5 for $Pr = 0.814$. Without a discrimination between the different arrays, a comparison between Nu_{wf} (Figure

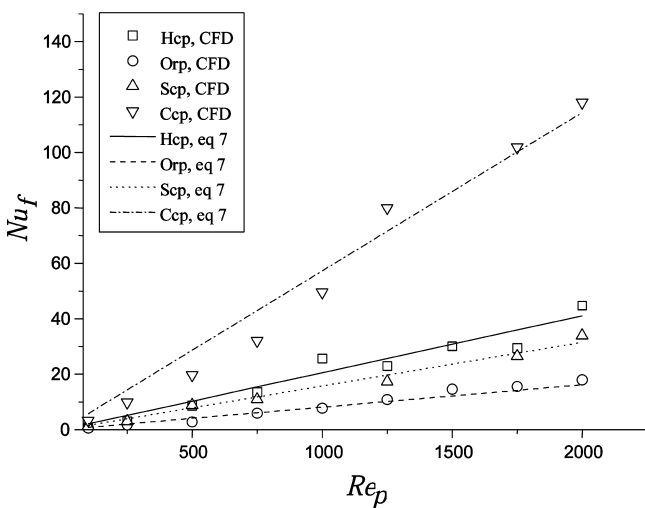


Figure 5. Nu_f versus Re_p values for different particles arrays.

3) and Nu_f (Figure 5) reveals that values of the latter are significantly lower, which means that the thermal resistance $1/h_f$ is indeed significant. The values of Nu_f for Orp and Hcp are on the lower side, a feature that can be attributed to the small size of the openings that connect the wall and core channels in the first particle layer. On average, the cubic arrays, Ccp and Scp, provide larger values of Nu_f . In particular, Nu_f for Ccp becomes even larger than Nu_{wf} in the high Re_p range. The difference between Nu_f values for Ccp and Scp reveals that, apart from the size of the openings in the first particle layer, another effect should be considered. For the Ccp, particles of the second layer deeply intrude between particles of the first layer, as is clearly appreciated in the “side view” presented in Figure 2. This feature promotes that the main streamlines between both particles layers pass closer to the openings at $D_p/2$, which thus enhances the heat exchange between the wall and core channels.

A similar effect explains the differences between Nu_f values of Hcp and Orp.

In an attempt to relate quantitatively the calculated values of Nu_f with the bed structure, the effect of the size of the openings has been accounted for by the wall-channel voidage ϵ_1 , and the just discussed effect of the intrusion of second layer particles into the first layer is evaluated by the difference $\epsilon_1 - \epsilon_c$. In this way, eq 7 has been employed to correlate the results:

$$Nu_f = A \epsilon_1^\alpha [1 + B(\epsilon_1 - \epsilon_c)] Re_p Pr \tag{7}$$

In a first step, Re_p and Pr were raised to fitting exponents, but after the adjusting procedure, both powers did not significantly depart from the unity. Considering that the thermal exchange mechanism between wall and core channels should be of convective nature, at least at the relatively high Reynolds numbers in the numerical experiments, it was decided to use the expression as in eq 7. Best values of the fitting parameters α, A, B , and their confidence intervals are

$$\alpha = 4 \pm 0.7, A = 0.346 \pm 0.05, B = 11.4 \pm 2.4$$

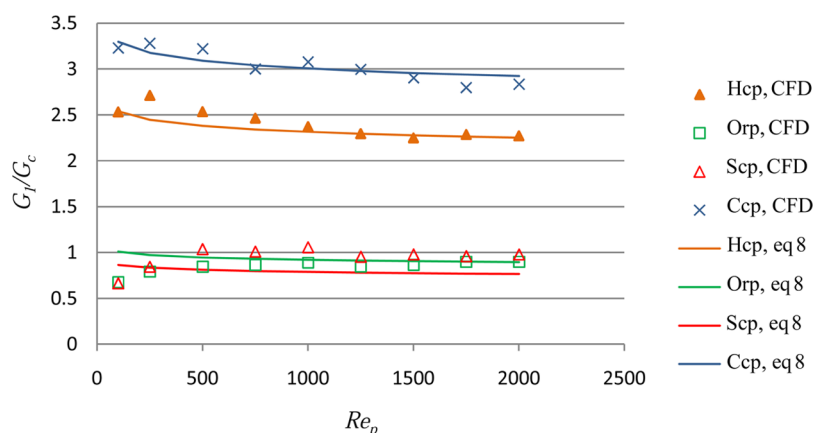


Figure 6. G_1/G_c versus Re_p values for different particle arrays (Figure 2).

The coefficient of determination was $R^2 = 0.989$. Figure 5 illustrates that eq 7 is able to fit correctly the available data of Nu_f .

4.3. Ratio G_1/G_c between Wall and Core Regions Superficial Mass Velocities. For a given value of the overall superficial mass velocity G , CFD simulations allow for evaluation of the ratio of mass velocities in the wall and core channels, G_1/G_c . Note that if S_1 is the fractional bed cross-section between the wall and a distance $D_p/2$, it follows that $SG = S_1G_1 + S_cG_c$, where S is the total bed cross-section and $S_c = S - S_1$.

The results are plotted in Figure 6 along with values from eq 8 described below. For the arrays in which $\varepsilon_1 = \varepsilon_c$ (Orp and Scp, Table 1), values $G_1/G_c < 1$ should arise due to the additional friction exerted by the wall. A couple of values for the Scp were, instead, slightly larger than one, which was ascribed to inaccuracies from velocity-field calculations and from the averaging procedure.

The Hcp and Ccp facilitate the flow in the wall region since ε_1 is significantly larger than ε_c , and hence $G_1/G_c > 1$. The CFD data in Figure 6 were correlated by means of eq 8:

$$G_1/G_c = A\varepsilon_1^\alpha \varepsilon_c^\gamma Re_p^\beta \quad (8)$$

Best values of the fitting parameters α , A , B , and their confidence intervals are

$$A = 0.55 \pm 0.01, \alpha = 1.5 \pm 0.3, \gamma = -2.4 \pm 0.2, \beta = -0.04 \pm 0.03$$

The coefficient of determination was $R^2 = 0.982$.

Equation 8 and its fitting parameters are expected to be applied for randomly packed beds in cylindrical vessels. According to our analysis of data for reasonably well compacted beds of monosized spheres and $5 < N < \infty$, ranges of voidages are $0.38 < \varepsilon_c < 0.41$ and $0.48 < \varepsilon_1 < 0.55$. From eq 8, an interval range of $1.2 < G_1/G_c < 1.8$ arises by assuming $Re_p = 500$. Values calculated for the regular arrays are either above or below that range (Figure 6). Therefore, although a comparison of present values of G_1/G_c with results from literature information is not within the scope of this manuscript, it seems relevant to check if data from randomly packed beds do lie in the range of $1.2 < G_1/G_c < 1.8$. Benham et al.⁶ presented results of radial velocity profiles from CFD evaluations in randomly packed beds of considerably large numbers of particles (up to ~ 800). For example, graphical results are presented for $Re_p = 450$, an aspect ratio $N = 8$ (a representative value of the range employed in commercial multitubular packed bed reactors say, $5 < N < 15$), along with the corresponding radial voidage profiles. From this information, we have evaluated $\varepsilon_1 = 0.544$, $\varepsilon_c = 0.398$, and $G_1/G_c = 1.57$. This

value lies well inside the aforementioned interval. Besides, with such values of Re_p , ε_1 , and ε_c , eq 8 predicts that $G_1/G_c = 1.62$, which compares quite satisfactorily with the value from Benham et al.⁶

5. COMPARISON OF COEFFICIENTS h_{wf} AND h_f WITH LITERATURE CORRELATIONS

In the vast majority of works that report bed-to-wall heat transfer experiments in randomly packed beds, the data were reduced according to the S2D model, and in this way a number of correlations for the S2D model's wall heat-transfer coefficient h_w^S are available. As discussed in the Introduction, h_w^S encloses a number of effects; hence, a comparison with values of the 2R2D model's parameters presented in this contribution cannot be made straightforwardly.

It should be recalled that available data and correlations for h_w^S are quite dispersed. This fact has been illustrated, for example, in the works of Li and Finlayson¹⁷ and Tsotsas and Schlünder,¹⁸ where it can be appreciated that differences of more than one order of magnitude arise for practical values of Re_p . Reasons for these discrepancies have been thoroughly discussed by Dixon.¹ Nonetheless, the author emphasized that the approach followed originally by Yagi and Kunii¹⁹ to express h_w^S values provides a good frame to rationalize the available information. As discussed next, this approach is also most useful to relate h_w^S to the heat-transfer coefficients h_{wf} and h_f evaluated in this contribution. The Yagi and Kunii¹⁹ formulation (in terms of Nusselt numbers) is

$$Nu_w^S = Nu_{w,0} + \frac{1}{1/Nu_w^* + 1/Nu_m} \quad (9)$$

Equation 9 adds heat-transfer contributions due to conductive ($Nu_{w,0}$) and convection (the second term on the right-hand side) mechanisms. Concerning the convective contribution, Yagi and Kunii¹⁹ identified the two thermal resistances that are conceived for the 2R2D model, that is, that of a "true" thermal film on the wall ($1/Nu_w^*$, in eq 9) and that caused by the restricted fluid dispersion at about $D_p/2$ ($1/Nu_m$ in eq 9). As they are serially located on the radial direction of heat transfer, it is also reasonable to add these two thermal resistances, as in eq 9, by assuming the same thermal flux through each of them.

However, this is an approximation since the effect of enthalpy change of the fluid flowing between the wall and the distance $D_p/2$ (i.e., in the wall channel of the 2R2D model) and that of the heat released by chemical reaction in this zone is disregarded. Instead, this is taken into account in the 2R2D model. In beds of

Table 2. Values of Parameters in Eq 9 and Features of Different Correlations for Nu_w^S

references	a	β	γ	type of experiments	relation with eq 9
Yagi and Wakao ²¹	0.2	0.80	1/3	heat transfer	$h_{w,0}, h_w^*, h_m$
Li and Finlayson ¹⁷	0.17	0.79	0	heat transfer	$h_{w,0}, h_w^*, h_m$
Peters et al. ²²	$4.9(1/N)^{0.26}$	0.5	1/3	heat transfer	$h_{w,0}, h_w^*, h_m$
Olbrich and Potter ²⁰	8.9	0.34	1/3	mass transfer/gas flow	h_w^*, h_m
Dixon and Labua ²³	$1-1/N$	0.61	1/3	mass transfer/liquid flow	h_w^*
Kunii et al. ²⁴	$0.06/\varepsilon_w^2$	0.75	1/3	mass transfer/liquid flow	h_w^*

large aspect ratios N , those effects will not be important, but in beds involved in multitubular reactors (say, $N < 10-15$), that zone conveys a relevant fraction of the overall flow, and significant differences in the behavior predicted by S2D and 2R2D models can arise as discussed by Asensio et al.² In spite of these observations, results of Nu_w^S expressed as in eq 9 can be employed in first approximation to compare values of h_w^* with $h_{w,f}$ and those of h_m with h_f . It is relevant to quote that Dixon¹ discussed subsequent efforts that employed eq 9 to reduce experimental data, and finally he recommended this expression to estimate the S2D model parameter Nu_w^S . For this end, Dixon¹ suggests employing

$$Nu_w^* = 0.3Re_p^{3/4}Pr^{1/3} \quad (10a)$$

$$Nu_m = 0.054Re_pPr \quad (10b)$$

Equation 10b is the same proposed originally by Yagi and Kunii.¹⁹

Many other correlations for Nu_w^S are of the empirical form:

$$Nu_w^S = aRe_p^\beta Pr^\gamma \quad (11)$$

This kind of expression has been employed to fit heat-transfer data, mostly with gas flow, and it has been also used (in terms of the analogous dimensionless numbers) to reduce experiments in which mass-transfer rates between the wall and flowing liquid streams were measured. The parameters of some of these expressions are given in Table 2. The correlation of Olbrich and Potter,²⁰ based on mass transfer experiments but with gas flow, is also included in Table 2. If we try to interpret expressions of the form in eq 11 in terms of the contributions discriminated in eq 9, all correlations based on heat-transfer experiments should include in some way the effect of the three coefficients $h_{w,0}$, h_w^* , and h_m .

However, for mass-transfer experiments, the contribution of $h_{w,0}$ is absent. Besides, as Prandtl numbers for liquids are of the order of 10^3 , h_m becomes much larger than h_w^* for usual Re_p numbers (e.g., when $Re_p = 100$, $Pr = 1000$, the results from eqs 10a and 10b are $h_w^* = 95$, $h_m = 5400$), and consequently it can be concluded that $Nu_w^S \approx Nu^*$ for mass-transfer experiments with liquid flow. Finally, in the correlation of Olbrich and Potter,²⁰ only $h_{w,0}$ can be disregarded. These observations are summarized in Table 2.

It follows that $Nu_{w,f}$ from eq 6 can be directly compared to the correlations of Kunii et al.,²⁴ Dixon and Labua,²³ and with values from eq 10a. Equation 6 needs values of ε_1 and ε_c to be fixed (through Re_{p1} and G_1/G_c , eq 8). In turn, ε_1 and ε_c depend on the aspect ratio N . To carry out the comparison, values in the range of $5 < N < 15$ were considered. From the relationships used by Asensio et al.,² the values in Table 3 arose. For the correlation of Kunii et al.,²⁴ it was assumed that $\varepsilon_w = \varepsilon_1$. Furthermore, the comparison is made for $Pr = 0.814$.

Table 3. Variables Employed in Figure 7

N	ε_1	ε_c	ε
5	0.507	0.397	0.436
15	0.484	0.380	0.393

Values of Nusselt numbers in Figure 7 for $N = 5$ show moderate differences. The values of $Nu_{w,f}$ from eq 6 are well inside the low and upper limits defined by the expressions of Nu_w^S and Nu_w^* in the whole range of $100 < Re_p < 2000$. Similar conclusions arise for higher values of N .

It was discussed before in this section that the coefficient h_m , according to eq 9, is conceptually comparable to the heat-exchange coefficient h_f evaluated in this work. Values of Nu_m from eq 10b and of Nu_f from eq 7 are plotted in Figure 8 for $Pr = 0.814$ and two values of $N = 5, 15$ (see Table 3). The agreement between Nu_m and Nu_f is very good, with nearly coincident values at $N = 5$.

For further analysis of the CFD results presented here ($h_{w,f}$, h_f and G_1/G_c), overall heat-transfer rates predicted by the 2R2D model can be compared with those predicted by the S2D model that employs values of h_w^S from the correlations in the literature. A suitable situation for such a comparison is established by considering the heat-exchange rates far from the bed inlet (i.e., when entrance effects vanish) between the fluid stream and the wall maintained at uniform temperature and disregarding any chemical reaction. In both models, the Bey and Eigenberger²⁵ expression for effective thermal conductivity is employed in the form $\lambda_{ef,c} = 0.1D_p c_{p,f} G_c$ for the 2R2D model and $\lambda_{ef} = 0.1D_p c_{p,f} G$ for the 2RD model. This choice helps to minimize the impact of thermal resistance in the bulk of the bed in the comparison. However, since this resistance will be controlling at large N , while the purpose of the comparison is to evaluate near-wall effects, an equivalent heat-transfer coefficient at the wall $h_w^{S,Eq}$ is calculated for the S2R model by matching its results of the overall heat-transfer rate and averaged temperature to those of the 2R2D model. The formulation to calculate $h_w^{S,Eq}$ is given in the Appendix C of Asensio et al.² Since only the convective contributions ($h_{w,f}$, h_f) are used in the 2R2D model to account for heat transfer in the near-wall region, the equivalent parameter $h_w^{S,Eq}$ does not include the particle-conductive contribution. Then, $Nu_w^{S,Eq}$ can be fairly compared to values from eq 9 if $Nu_{w,0}$ is dropped, that is:

$$Nu_w^S = \frac{1}{1/Nu_w^* + 1/Nu_m} \quad (12)$$

$Nu_w^{S,Eq}$ at $N = 5$ is compared in Figure 9 to values of Nu_w^S from eq 12 and from eq 11 with parameters from the first four references in Table 2. By recalling the mechanisms represented by Olbrich and Potter²⁰ parameters (Table 2), a one-to-one comparison with $Nu_w^{S,Eq}$ can be made. For the remaining three references in Table 2, it is recalled that eq 11 includes implicitly the contribution $Nu_{w,0}$.

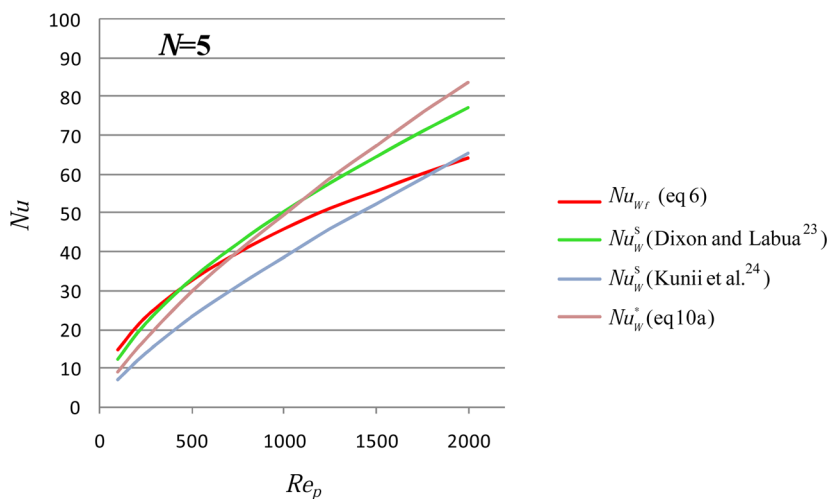


Figure 7. Comparison among Nu_w^S (mass transfer/liquid flow, see Table 2), Nu_w^* (eq 10a), and Nu_{wf} (eq 6) at $Pr = 0.814$, $N = 5$.

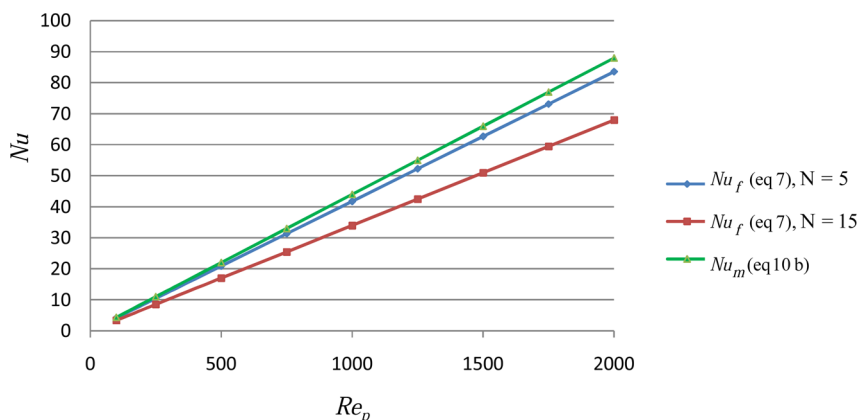


Figure 8. Comparison between Nu_m (eq 10b) and Nu_f (eq 7) values at $Pr = 0.814$.

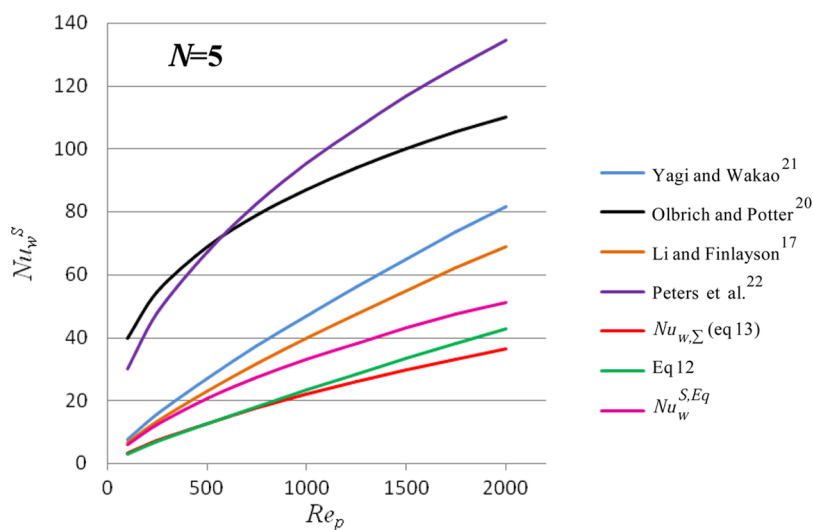


Figure 9. Comparison of expressions for Nu_w^S , $Pr = 0.814$, $N = 5$.

The final set of values plotted in Figure 9 corresponds to

$$Nu_{w,\Sigma} = \frac{1}{1/Nu_{wf} + 1/Nu_f} \tag{13}$$

where Nu_{wf} and Nu_f are evaluated from eqs 6 and 7. $Nu_{w,\Sigma}$ is formulated in eq 13 by following the same reasoning as described

for eq 9 but with the individual thermal resistances evaluated from the present results. By recalling the observation made at the beginning of this section, differences between $Nu_w^{S,Eq}$ and $Nu_{w,\Sigma}$ should be mainly ascribed to the effect of the fluid flow in the wall channel of the 2R2D model. $Nu_{w,\Sigma}$ has been included in Figure 9 to evaluate such effect.

The dispersion of literature data for Nu_w^S is evident in Figure 9. Values from the four correlations (Table 2) expressed by eq 11 are definitely larger than $Nu_w^{S,Eq}$ and those from eq 12. However, by considering values of $8 < Nu_{w,0} < 25$, as employed by Tobis and Ziolkowski,²⁶ and adding $Nu_{w,0}$ to both $Nu_w^{S,Eq}$ and Nu_w^S from eq 12, values close to the correlations of Yagi and Wakao²¹ and Li and Finlayson¹⁷ arise. Instead, the high values from the correlations of Olbrich and Potter²⁰ and Peters et al.²² cannot be approached in this way.

A reasonable agreement between $Nu_w^{S,Eq}$ and Nu_w^S from eq 12 can be appreciated in Figure 9, and differences become even smaller at higher values of N . This result is most relevant to validate the procedure undertaken in this contribution for the evaluation of the 2R2D model's parameters if we recall that eq 9, and hence eq 12, has been recommended from a critical revision of the existing literature information.¹

The comparison between $Nu_w^{S,Eq}$ and $Nu_{w,\Sigma}$ deserves a final comment. At $N = 5$ (Figure 9), the differences between them reveal that effectively the fluid flow in the wall region enhances the heat-transfer rate ($Nu_w^{S,Eq} > Nu_{w,\Sigma}$). This effect explains why, on average, $Nu_w^* > Nu_{wf}$ and $Nu_m > Nu_f$ hold in Figures 7 and 8, while for the overall coefficients in Figure 9, the reverse trend clearly holds: Nu_w^S (eq 12) $<$ $Nu_w^{S,Eq}$. It should be noted that at larger values of N , the effect of the fluid flow in the wall region weakens but remains noticeable at least up to around $N = 15$.

6. CONCLUSIONS

The 2R2D model recently proposed by Asensio et al.² identifies a wall channel, from the wall up to a distance $D_p/2$, in which the fluid stream exchanges heat with the wall through an actual thermal film (heat-transfer coefficient h_{wf}), while heat exchange with the core channel (extended from $D_p/2$ up to the bed axis) is limited by a highly restrained fluid motion at distances of around $D_p/2$. The heat-exchange rate between both channels is based on an effective heat-exchange coefficient h_f .

CFD simulations aimed to evaluate h_{wf} , h_f and the ratio between superficial mass velocities in both channels G_1/G_c have been reported here. Four regular arrays of spheres between parallel planes were employed to this end. These arrays provide different combinations of wall and core channel voidages, ε_1 and ε_c , which are regarded as being the basic structural parameters on which h_{wf} , h_f and G_1/G_c will depend. Reynolds and Prandtl numbers were covered in the ranges of $100 < Re_p < 2000$ and $0.4 < Pr < 3.5$ (gases). The results of h_{wf} and h_f were well correlated with ε_1 , ε_c , Re_p , and Pr (eqs 6 and 7) and those of G_1/G_c with ε_1 , ε_c and Re_p (eq 8).

Section 5 of this contribution describes a first attempt to test the applicability of the results of h_{wf} and h_f for randomly packed beds. To this end, values of ε_1 and ε_c typical of randomly packed beds in the range of $5 < N < 15$ were employed in the expressions developed for h_{wf} and h_f . A number of correlations for the S2D model's coefficient h_w^S are available in the literature, but results for the individual parameters h_{wf} and h_f are not directly available with exception made of the expression recommended by Dixon's¹ review. In this case, the heat-transfer contributions in h_w^S are disaggregated, and particularly the fluid convection contribution is expressed in terms of an addition of two resistances that conceptually correspond to $1/h_{wf}$ and $1/h_f$. Although for the 2R2D model such thermal resistances do not operate strictly in series, values of each of them from both models can be expected to be closely related, and this is found to effectively happen for h_f . Regarding h_{wf} , the comparison made could include data from experiments of liquid-phase mass

transfer to the wall since in this case, the only relevant resistance, by analogy, corresponds to $1/h_{wf}$. Values of h_{wf} estimated in this contribution turned out to be inside the limits of variation defined by the experimental values from the different sources, and they are particularly close to values from the correlation recommended by Dixon.¹ A final comparison between the results of the present contribution with experimental results could be achieved by analyzing the heat-transfer rates predicted from the 2R2D model using values of h_{wf} , h_f and G_1/G_c here evaluated and from the S2D model that employs literature correlations for h_w^S . It could be concluded that results compared quite well when the S2D model is used with values of h_w^S from the expression recommended by Dixon,¹ and by taking due account of particle conduction effects, a reasonable agreement is also found with some of the remaining correlations.

Altogether, values of the 2R2D model's thermal parameters h_{wf} and h_f evaluated from CFD simulations seem to be in good agreement with experimental results. CFD simulations for randomly packed beds are currently under way with the purpose of adding further support for the results reported herein.

AUTHOR INFORMATION

Corresponding Author

*E-mail: german.mazza@probiem.gov.ar.

Notes

The authors declare no competing financial interest.

ACKNOWLEDGMENTS

The authors wish to thank the Universidad Nacional de La Plata (PID 11/I177), Universidad Nacional del Comahue (PID 04/I191), ANPCyT (PICT11-1641), ANPCyT, PRH 33, and CONICET (PIP 0304) for providing financial support. G.D.M. and G.F.B. are research members of CONICET (Argentina).

NOMENCLATURE

- c_{pf} = specific heat of the fluid, J kg⁻¹ K⁻¹
- D_t = tube diameter, m
- D_p = particle diameter, m
- G = specific mass flow rate (generic or average on the bed cross-section), kg m⁻² s⁻¹
- H = cell height in CFD simulations, m
- h_f = heat exchange coefficient between the wall and core channels (2R2D model), W m⁻² K⁻¹
- h_w^* = heat transfer coefficient across the thermal film on the wall (eqs 9 and 10a), W m⁻² K⁻¹
- h_m = heat transfer coefficient across bed restrictions at $D_p/2$ (eqs 9 and 10b), W m⁻² K⁻¹
- h_w^S = wall-to-bed heat transfer coefficient in S2D model, W m⁻² K⁻¹
- $h_{w,0}$ = wall-to-bed heat transfer coefficient due to conductive contributions, W m⁻² K⁻¹
- $h_w^{S,Eq}$ = wall-to-bed heat transfer coefficient in S2D model, evaluated from the 2R2D model, W m⁻² K⁻¹
- h_{wf} = heat transfer coefficient across the thermal film on the wall (2R2D model), W m⁻² K⁻¹
- N = tube-to-particle diameter ratio ($= D_t/D_p$)
- Nu = Nusselt number (suffix is that of the heat transfer coefficient h) ($= hD_p/\lambda_f$)
- $Nu_{w,\Sigma}$ = Nusselt number calculated with eq 13
- Pr = Prandtl number ($= c_{pf} \mu_f / \lambda_f$)
- Q_w = heat flux at the wall, W m⁻²
- Re_p = Reynolds number ($= G D_p/\mu_f$)

S = cross-sectional area, m^2
 T = fluid phase temperature, K
 $T_{c,l}$ = temperature in the core channel at the boundary with the wall channel, K
 T_w = wall surface temperature, K
 W = width of the bed, m
 y = distance from the wall surface, m
 x = Cartesian coordinate normal to y and z , m
 z = axial coordinate, m

Greek Symbols

ε = void fraction (generic or average on the bed cross section)
 λ_e = effective radial thermal conductivity of the bed, $W\ m^{-1}\ K^{-1}$
 λ_{ef} = contribution of fluid to λ_e , $W\ m^{-1}\ K^{-1}$
 λ_f = fluid thermal conductivity, $W\ m^{-1}\ K^{-1}$
 μ_f = fluid viscosity, $kg\ m^{-1}\ s^{-1}$

Subscripts and Superscripts

l = average quantity evaluated in $0 < y < D_p/2$
 c = relative to the core channel
 w = quantity evaluated at the tube wall

REFERENCES

- (1) Dixon, A. G. Fixed Bed Catalytic Reactor Modeling—The Radial Heat Transfer Problem. *Can. J. Chem. Eng.* **2012**, *90*, 507.
- (2) Asensio, D. A.; Zambon, M. T.; Mazza, G. D.; Barreto, G. F. Heterogeneous Two-Region Model for Low-Aspect-Ratio Fixed-Bed Catalytic Reactors. Analysis of Fluid-Convective Contributions. *Ind. Eng. Chem. Res.* **2014**, *53*, 3587.
- (3) Zhang, W.; Thompson, K. E.; Reed, A. H.; Beenken, L. Relationship between Packing Structure and Porosity in Fixed Beds of Equilateral Cylindrical Particles. *Chem. Eng. Sci.* **2006**, *61*, 8060.
- (4) Marek, M. Numerical Generation of a Fixed-Bed Structure. *Chem. Process Eng.* **2013**, *34*, 347.
- (5) Dixon, A. G.; Nijemeisland, M.; Stitt, E. H. Packed Tubular Reactor Modeling and Catalyst Design Using Computational Fluid Dynamics. *Adv. Chem. Eng.* **2006**, *31*, 307.
- (6) Behnam, M.; Dixon, A. G.; Nijemeisland, M.; Stitt, E. H. A New Approach to Fixed-Bed Radial Heat-Transfer Modeling Using Velocity Fields from CFD Simulations. *Ind. Eng. Chem. Res.* **2013**, *52*, 15244.
- (7) Romkers, S.; Dautzenberg, F.; van den Bleek, C. M.; Calis, H. CFD Modelling and Experimental Validation of Particle-to-Fluid Mass and Heat Transfer in a Packed Bed at Very Low Channel-to-Particle Diameter Ratio. *Chem. Eng. J.* **2003**, *96*, 3.
- (8) Nijemeisland, M.; Dixon, A. G. CFD Study of Fluid Flow and Wall Heat Transfer in a Fixed Bed of Spheres. *AIChE J.* **2004**, *50*, 906.
- (9) Guardo, A.; Coussirat, M.; Larrayoz, M. A.; Recasens, F.; Eguisquiza, E. Influence of the Turbulence Model in CFD Modeling of Wall-to-Fluid Heat Transfer in Packed Beds. *Chem. Eng. Sci.* **2005**, *60*, 1733.
- (10) Magnico, P. Pore-Scale Simulations of Unsteady Flow and Heat Transfer in Tubular Fixed Beds. *AIChE J.* **2009**, *55*, 849.
- (11) Dixon, A. G.; Walls, G.; Stanness, H.; Nijemeisland, M.; Stitt, E. H. Experimental Validation of High Reynolds Number CFD Simulations of Heat Transfer in a Pilot-Scale Fixed-Bed Tube. *Chem. Eng. J.* **2012**, *200–202*, 344.
- (12) Zambon, M. T. Modeling of Heat Transfer in Low-Aspect-Ratio Fixed-Bed Reactors Assisted by CFD. Ph.D. Thesis, University of La Plata, La Plata, Argentina, 2010.
- (13) Dixon, A. G.; Nijemeisland, M.; Stitt, E. H. Systematic Mesh Development for 3D CFD Simulation of Fixed Beds: Contact Points Study. *Comput. Chem. Eng.* **2013**, *48*, 135.
- (14) Calis, H. P.; Nijenhuis, A. J.; Paikert, B. C.; Dautzenberg, F. M.; van den Bleek, C. M. CFD Modeling and Experimental Validation of Pressure Drop and Flow Profile in a Novel Structured Catalytic Reactor Packing. *Chem. Eng. Sci.* **2001**, *56*, 1713.
- (15) Nijemeisland, M.; Dixon, A. G. Comparison of CFD Simulations to Experiment for Convective Heat Transfer in a Gas–Solid Fixed Bed. *Chem. Eng. J.* **2001**, *82*, 231.
- (16) Bai, H.; Theuerkauf, J.; Gillis, P. A Coupled DEM and CFD Simulation of Flow Field and Pressure Drop in Fixed-Bed Reactor with Randomly Packed Catalyst Particles. *Ind. Eng. Chem. Res.* **2009**, *48*, 4060.
- (17) Li, C.; Finlayson, B. A. Heat Transfer in Packed Beds—A Reevaluation. *Chem. Eng. Sci.* **1997**, *32*, 1055.
- (18) Tsotsas, E.; Schlünder, E.-U. Heat Transfer in Packed Beds with Fluid Flow Remarks on the Meaning and the Calculation of a Heat-Transfer Coefficient at the Wall. *Chem. Eng. Sci.* **1990**, *45*, 819.
- (19) Yagi, S.; Kunii, D. Studies on Heat Transfer Near Wall Surface in Packed Beds. *AIChE J.* **1960**, *6*, 97.
- (20) Olbrich, W.; Potter, O. Mass Transfer from the Wall in Small-Diameter Packed Beds. *Chem. Eng. Sci.* **1972**, *27*, 1733.
- (21) Yagi, S.; Wakao, N. Heat and Mass Transfer from Wall to Fluid in Packed Beds. *AIChE J.* **1959**, *5*, 79.
- (22) Peters, P. E.; Schiffino, R. S.; Harriot, P. Heat Transfer in Packed-Tube Reactors. *Ind. Eng. Chem. Res.* **1998**, *27*, 226.
- (23) Dixon, A. G.; Labua, L. A. Wall-to-Fluid Coefficients for Fixed-Bed Heat and Mass Transfer. *Int. J. Heat Mass Transfer* **1985**, *28*, 879.
- (24) Kunii, D.; Suzuki, M.; Ono, N. Heat Transfer from Wall Surface to Packed Beds at High Reynolds Number. *J. Chem. Eng. Jpn.* **1968**, *1*, 21.
- (25) Bey, O.; Eigenberger, G. Gas Flow and Heat Transfer through Catalyst-Filled Tubes. *Int. J. Therm. Sci.* **2001**, *40*, 152.
- (26) Tobiš, J.; Ziolkowski, D. Modelling of Heat Transfer at the Wall of a Packed-Bed Apparatus. *Chem. Eng. Sci.* **1988**, *43*, 3031.